

Solitonic Andreev Spin Qubit

Pablo San-Jose^{1,*} and Elsa Prada¹

¹*Instituto de Ciencia de Materiales de Madrid (ICMM), CSIC, Madrid, Spain*

(Dated: June 23, 2025)

We propose a novel type of superconducting spin qubit, dubbed solitonic Andreev spin qubit (SASQ), that combines features of Andreev spin qubits and geometric spin qubits. The two SASQ states are the degenerate spin orientations of an Andreev bound state trapped in a circular Josephson junction with a Corbino disk geometry, created on a 2DEG. The junction is subjected to a weak magnetic flux that induces a fluxoid mismatch between the inner disk and outer ring superconductors. The fluxoid mismatch produces a cancellation of the induced pairing that traps unconventional spin-degenerate Andreev bound states analogous to Jackiw-Rebbi soliton states. They are localized at a position around the junction that can be controlled by changing the superconducting phase difference. Moving a soliton state with a phase bias induces a holonomic rotation of its spin, by virtue of the spin-orbit coupling in the 2DEG. The holonomic qubit trajectories can densely cover the full Bloch sphere as the soliton state revolves around the junction. Effects of non-holonomic (dynamic) qubit drift are also analyzed.

Qubit design plays a central role in our efforts to build a practical and universal quantum computer. The design space for qubits is very large, with many factors affecting the future prospects of each qubit class. While many of the leading quantum computers currently available are based on variations of the superconducting (SC) transmon qubit [1, 2], it is believed that optimally scalable quantum architectures will probably require different qubit designs with less control hardware [3] and that allow for more efficient error correction schemes. Majorana-based topological qubits [4–6] or cat-state qubits [7, 8] are prime examples of the latter. Many other types of physical qubit implementations are being intensively investigated [9–14]. Some recent designs, such as the Kitaev-Sau chain [15, 16] or the Andreev spin qubit (ASQ) [17, 18], combine ingredients from several previous qubit ideas to circumvent some limitations.

The ASQ in particular is based on the original quantum-dot spin qubit proposal [19], where the spin in a quantum dot is manipulated coherently using Zeeman fields or nanomagnets. The ASQ concept replaces these problematic magnetic elements by the SC phase difference (or a supercurrent) across a Josephson junction (JJ) with the quantum dot inside, see Fig. 1(a). Fully controlling the spin qubit this way is made possible by electrostatic gating and the presence of spin-orbit (SO) coupling in the quantum dot. An unrelated and beautiful variation of the traditional spin qubit, also reliant on SO coupling to remove the need of magnetic fields, is the geometric spin qubit (GSQ) concept, in which the quantum dot is able to move within its two-dimensional electron gas (2DEG) host, see Fig. 1(b). Arbitrary manipulations of the spin in a GSQ is achieved without any magnetic fields by real-space displacements of the dot center along a path \mathcal{C} in the presence of SO coupling [20–23]. This kind of manipulation is an example of a holonomic quantum gate [24–26], which is characterized by

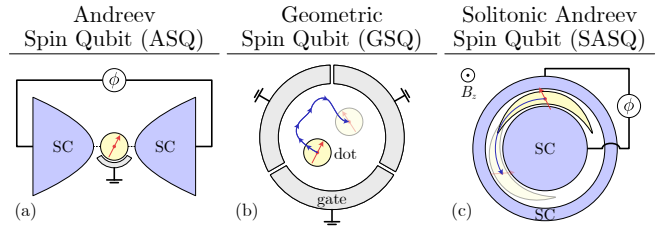


FIG. 1. The solitonic Andreev spin qubit (c) combines elements from the Andreev spin qubit (a) and the geometric spin qubit (b). It is controlled with a phase bias ϕ like the former and allows holonomic operations like the latter. In (c), superconducting regions (blue) form a Corbino Josephson junction on a 2DEG (white). The junction is subjected to a weak magnetic field B_z to induce a fluxoid mismatch between the inner disk and the outer ring. This creates a solitonic Andreev state (yellow) that is spin-degenerate, and whose position can be tuned through ϕ . Moving the soliton state induces holonomic qubit rotations due to the spin-orbit coupling in the 2DEG.

being independent of manipulation timing (as long as it is sufficiently slow), depending purely on the geometry of \mathcal{C} instead. This removes one source of fidelity-reducing noise [27], and makes inverting a single-qubit gate easier in principle. However, since possible displacements are often small, with \mathcal{C} often bounded within a small region of the 2DEG, the maximum speed of GSQ operations is strongly reduced.

In this work we propose a new type of qubit design, dubbed solitonic Andreev spin qubit (SASQ), that combines features from the GSQ and the ASQ, see Fig. 1(c). Like in ASQs, single-qubit operations are performed by controlling the SC phase difference across a special kind of JJ. Unlike in the ASQ, however, the induced operation is holonomic. Compared to a GSQ, the possible displacements can be arbitrarily large, so that the holonomic qubit operations may be far more efficient, even with a weak SO coupling. The basic elements of the SASQ are the following: (a) a Corbino JJ, fabricated by epitax-

* pablo.sanjose@csic.es

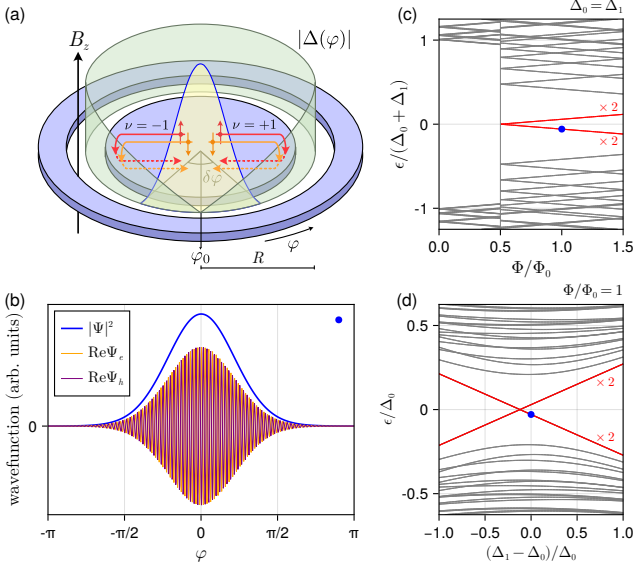


FIG. 2. (a) Sketch of the solitonic Andreev bound states (yellow) concentrated at radius R within an angular spread $\delta\varphi$ from the minimum of the total pairing $|\Delta(\varphi)|$ (green) at φ_0 . The $\Delta(\varphi)$ profile, Eq. (2), results from a different fluxoid number in the inner disk (zero) and the outer ring (one) produced by a flux $\Phi = \pi R^2 B_z$ between $0.5\Phi_0$ and $1.5\Phi_0$, where Φ_0 is the SC flux quantum. There are two spinful low-energy pairs of such states of opposite energy around $\nu \pm 1$ Fermi points. Their analytical wavefunction [without SO coupling, Eq. (3)] is shown in (b) for $\Phi/\Phi_0 = 1$ and $\Delta_0 = \Delta_1$, where Δ_0 and Δ_1 are the pairing amplitudes from the disk and ring. Their corresponding energy versus Φ/Φ_0 and versus pairing asymmetry $\Delta_0 - \Delta_1$ (at fixed $\Delta_0 + \Delta_1$) is shown in red in (c) and (d), respectively, where the rest of the spectrum is shown in gray.

ial deposition of an inner SC disk and an outer SC ring on a 2DEG with SO coupling; (b) a weak magnetic out-of-plane field B_z such that the flux threading the outer ring is around one flux quantum; and (c) a SC phase bias ϕ between the disk and ring, which can be tuned either with an external SQUID loop or by an electric bias $V(t) = \dot{\phi}(t)/2e$ across the junction. These ingredients give rise to the emergence of a special type of solitonic Andreev bound state in the circular junction region between disk and ring. The soliton state is centered around angle $\varphi_0 = \pi - \phi$ with a finite angular spread $\delta\varphi$. Its angular confinement is the result of a mismatch between the SC phase winding number of the disk and the ring, caused by the magnetic flux. The soliton bound state is spin-degenerate and implements a spin qubit when the junction is tuned to odd occupancy. The SASQ state can be controlled holonomically by moving the soliton state around the junction by varying the SC phase difference ϕ . We show that the full Bloch sphere can be covered in this way by slightly adjusting the effective SO length λ_{SO}^{-1} through the junction density.

Model.—A minimal model for the Corbino JJ can be

obtained by integrating out the gapped SC regions surrounding the junction region. The latter is modeled as a circular electron gas ring of radius R and polar coordinate φ , see Fig. 1(c). We consider that the 2DEG has Fermi velocity v_F , Fermi momentum k_F and a Rashba term $H_{\text{SO}} = \alpha(k_y\sigma_x - k_x\sigma_y)$, where α is the Rashba coupling, σ_i are Pauli matrices and \mathbf{k} is momentum (we take $\hbar = e = 1$ throughout). If we linearize the dispersion around the two Fermi momenta $\pm k_F$ along φ , we can write an effective Bogoliubov-de Gennes Hamiltonian [28] around each Fermi point $\nu = \pm 1$ as

$$\begin{aligned} H_\nu &= \begin{pmatrix} H_\nu^{\uparrow\uparrow} & H_\nu^{\uparrow\downarrow} \\ H_\nu^{\downarrow\uparrow} & H_\nu^{\downarrow\downarrow} \end{pmatrix}, \\ H_\nu^{\sigma\sigma} &= \begin{pmatrix} v_F(\nu k_\varphi - k_F - \nu A_\varphi) & \sigma\Delta(\varphi) \\ \sigma\Delta(\varphi)^* & -v_F(\nu k_\varphi - k_F + \nu A_\varphi) \end{pmatrix}, \\ H_\nu^{\uparrow\downarrow} &= (H_\nu^{\downarrow\uparrow})^\dagger = \begin{pmatrix} \alpha e^{i\varphi} k_\varphi & 0 \\ 0 & \alpha e^{-i\varphi} k_\varphi \end{pmatrix}. \end{aligned} \quad (1)$$

The Nambu basis $\check{c}^\dagger = (c_\uparrow^\dagger, c_\downarrow^\dagger, c_\downarrow, c_\uparrow)$ is chosen. Here $\sigma = \pm 1$ denotes spins \uparrow, \downarrow , $k_\varphi = \frac{1}{R}(-i\partial_\varphi)$ denotes the momentum around the junction, and $A_\varphi = RB_z/2$ is the vector potential in the symmetric gauge along the φ direction at radial position R for a uniform magnetic field B_z . The total pairing $\Delta(\varphi)$ induced from the disk and ring onto the junction region under the magnetic flux reads

$$\Delta(\varphi) = \Delta_0 + \Delta_1 e^{i\varphi} e^{i\phi} = \Delta_0 - \Delta_1 e^{i(\varphi - \varphi_0)}, \quad (2)$$

where $\varphi_0 = \pi - \phi$. Here, Δ_0 and Δ_1 are real pairing potentials induced on the junction by the disk and ring superconductors, respectively. We assume that the order parameter in the disk is real, while in the ring it has a φ -dependent phase $e^{in\varphi} e^{i\phi}$, where ϕ is the phase bias with respect to the disk and $n = \lfloor \Phi/\Phi_0 \rfloor = 1$ represents a flux-induced winding number, or *fluxoid*, in the ring. Here $\Phi = \pi R^2 B_z$ is the flux threading the junction and $\Phi_0 = h/2e$ is the SC flux quantum [29]. Fluxoid quantization was first predicted by London in multiply-connected superconductors threaded by a flux [30, 31]. The combination of the two pairings with different windings ($n = 0$ disk, $n = 1$ ring) results in a vanishing $\Delta(\varphi)$ at φ_0 if $\Delta_0 = \Delta_1$, see Fig. 2(a). More precisely $\Delta(\varphi) = (\Delta_0 - \Delta_1) + i(\varphi - \varphi_0)\Delta_1 + \mathcal{O}[(\varphi - \varphi_0)^2]$ [32].

Exact solution.—The model in Eq. (1) has two spin-degenerate Andreev bound states $|\Psi_{\nu\sigma}^0\rangle$ per Fermi point ν close to zero energy. They are spatially localized around φ_0 , as represented in Fig. 2(a). In the special case of $\Delta_0 = \Delta_1$ and $\alpha = 0$, these are also the lowest-energy eigenstate of the 2×2 $H_\nu^{\sigma\sigma}$ block, which allows us to find an exact analytical expression for their wavefunction and energy:

$$\begin{aligned} \langle \varphi | \Psi_{\nu\sigma} \rangle &= C e^{-\frac{1}{2} \frac{(4 \sin \frac{\varphi - \varphi_0}{4})^2}{\delta\varphi^2}} \begin{pmatrix} \sigma e^{i(\varphi - \varphi_0)(\nu k_F R + 1/4)} \\ \nu e^{i(\varphi - \varphi_0)(\nu k_F R - 1/4)} \end{pmatrix}, \\ \epsilon_\nu &= -\frac{\nu v_F}{2R} \left(\frac{\Phi}{\Phi_0} - \frac{1}{2} \right). \end{aligned} \quad (3)$$

Here $\delta\varphi = \sqrt{v_F/(R\Delta_1)} = \sqrt{\xi/R}$, ξ is the coherence length, and C is a normalization constant. A typical wavefunction is represented in Fig. 2(b), and the eigenenergy as a function of Φ is shown in red in Fig. 2(c). Higher excitations, computed numerically, are shown in gray [33].

The effect of a finite $\Delta_0 - \Delta_1$ can be computed in perturbation theory. It does not break the spin degeneracy, and simply amounts to an energy shift, with no change to eigenstates,

$$\begin{aligned} \delta\epsilon_\nu^\Delta &= (\Delta_0 - \Delta_1)\nu\gamma, \\ \gamma &= \frac{\int_{-\pi}^{\pi} d\varphi e^{-(4\sin\frac{\varphi}{4})^2/\delta\varphi^2} \cos\frac{\varphi}{2}}{\int_{-\pi}^{\pi} d\varphi e^{-(4\sin\frac{\varphi}{4})^2/\delta\varphi^2}} = \\ &= \frac{I_1(8/\delta\varphi^2) + L_{-1}(8/\delta\varphi^2)}{I_0(8/\delta\varphi^2) + L_0(8/\delta\varphi^2)}, \end{aligned} \quad (4)$$

$$(5)$$

where I_n and L_n are the n -th order modified Bessel function of the first kind and the modified Struve function. The expression for γ reduces to 1 and $2/\pi$ in the limits of small and large $\delta\varphi$, respectively. The eigenenergies, computed numerically as a function of $\Delta_1 - \Delta_0$, are shown in red in Fig. 2(d), which show that perturbation theory is accurate. A similar perturbative calculation for the SO coupling yields zero change of the eigenenergies to first order in α (although the eigenstates do change). Spin degeneracy is thus preserved at this level.

Several important aspects of the solution in Eq. (3) stand out: (1) the eigenstates are peaked around φ_0 , with an angular width given by $\delta\varphi$; (2) the wavefunction for a given σ and ν has Majorana character [34, 35]; (3) the two $\sigma = \pm 1$ excitations within each ν sector are degenerate, since ϵ_ν is independent of σ , while states from opposite Fermi points $\nu = \pm 1$ have opposite energy; (4) the energy is also independent of φ_0 (and hence of phase bias ϕ) and of Fermi momentum k_F ; (5) the energy vanishes as Φ/Φ_0 approaches 0.5 from above; (6) the low-energy Andreev levels are well separated spectrally from higher excitations, with a spacing that closely resembles the square-root dependence of Landau levels in graphene, see Fig. 2(b) around $\Phi/\Phi_0 \approx 0.5$.

The latter observation is not a coincidence. In fact, an intriguing interpretation of these states can be found by connecting the SASQ model to the problem of Dirac fermions in two dimensions. By expanding around $\varphi = \varphi_0$, we can map H_ν^σ to the 2D Dirac Hamiltonian (i.e. low-energy graphene) with a position-dependent mass term that changes sign at a boundary (a so-called scalar field soliton). This is a 2D version of the celebrated Jackiw-Rebbi problem [36]. It admits topological fermion states confined to the boundary by virtue of the opposite valley Chern number on each side. In the mapping to the graphene version, σ plays the role of spin, ν becomes valley, ϵ_ν is its Dirac point energy, electron/hole is the pseudospin, $(\Delta_0 - \Delta_1)/v_F$ is the momentum along the boundary, and $(\varphi - \varphi_0)\Delta_1$ is the position-dependent mass term, with φ_0 the position of the boundary. The map-

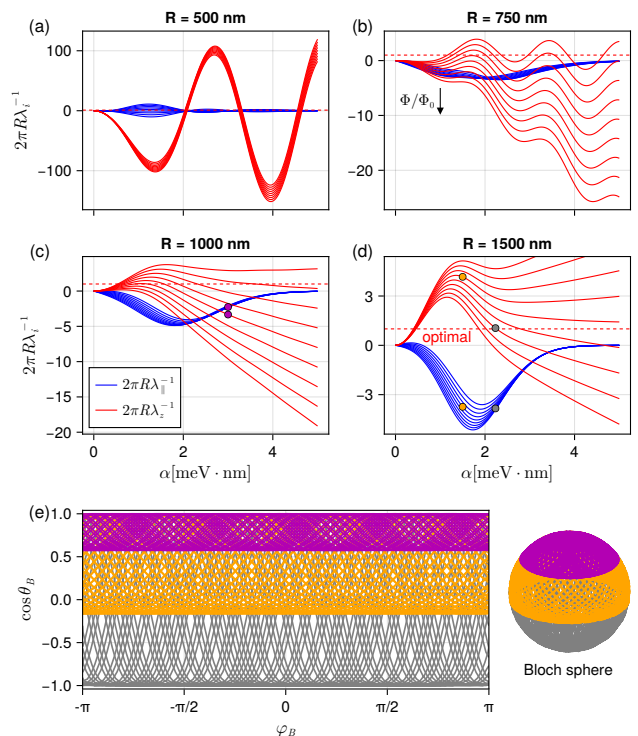


FIG. 3. The two components of the inverse spin-orbit length (in-plane λ_{\parallel}^{-1} in blue and out of plane λ_z^{-1} in red), normalized to the SASQ perimeter $2\pi R$ for four different radii R , are shown in (a-d). Different curves correspond to growing values of normalized flux Φ/Φ_0 from 0.6 to 1.4 in steps of 0.1. The holonomic evolution of the SASQ as the soliton state makes 20 turns around the junction is shown in (e) for three different values of α and Φ colored points in (c-d). A large fraction of the Bloch sphere, parametrized by angles θ_B and φ_B , is covered by the SASQ evolution, with full coverage (gray trajectory) achieved at the optimal point $2\pi R\lambda_z^{-1} = 1$ [dashed red line in (a-c)].

ping allows us to interpret the $|\Psi_{\nu\sigma}\rangle$ states as solitonic Jackiw-Rebbi solutions, whose existence is topologically dictated by the bulk-boundary correspondence principle, and does not require the small $\varphi - \varphi_0$ expansion used in the argument above.

Holonomic single-qubit gate.—Tuning the JJ to an odd occupancy state makes $|\Psi_{\nu\sigma}\rangle$ with $\epsilon_\nu < 0$ the twofold degenerate ground state of the system, which constitutes a SASQ. To perform a single-qubit operation on it, we can exploit the same principle as in GSQs by tuning position φ_0 through ϕ , from an initial φ_a to a final φ_b . The qubit rotation U reads $U = \text{Pexp}\left(-\frac{i}{2} \int_{\varphi_a}^{\varphi_b} d\varphi_0 2\pi R \lambda_{\text{SO}}^{-1}(\varphi_0) \cdot \boldsymbol{\sigma}\right)$ [22, 37, 38], Pexp is the path-ordered exponential and vector $\lambda_{\text{SO}}^{-1}(\varphi_0)$ is

$$\begin{aligned} \lambda_{\text{SO}}^{-1}(\varphi_0) &= \left(\lambda_{\parallel}^{-1} \cos \varphi_0, \lambda_{\parallel}^{-1} \sin \varphi_0, \lambda_z^{-1}\right) \\ &= \frac{1}{2\pi} \sum_{\sigma\sigma'} \langle \Psi_{\nu\sigma'} | k_\varphi | \Psi_{\nu\sigma} \rangle \boldsymbol{\sigma}_{\sigma\sigma'}. \end{aligned} \quad (6)$$

The inverse SO lengths λ_{\parallel}^{-1} and λ_z^{-1} for the soliton state must be computed numerically using the full Andreev wavefunctions with a finite α . The result, normalized to the junction circumference $2\pi R$, is shown in Fig. 3(a-d) for increasing junction radius R . The $2\pi R\lambda_{\parallel,z}^{-1}$ ratios are found to depend strongly on R , α and Φ , reaching large values even for modest SO coupling below 5 meV nm.

The number of rotations in the SASQ Bloch sphere after increasing φ_0 by 2π (one turn around the disk) is of the order of $2\pi R|\lambda_{\text{SO}}^{-1}|$, but the precise path in the Bloch sphere is complicated. Figure 3(e) shows typical qubit paths, evolving from $|\uparrow\rangle = (1, 0)$ to $(\cos(\theta_B/2), \sin(\theta_B/2)e^{i\varphi_B})$ in the Bloch sphere as the soliton state makes 20 full turns around the junction. We find that by slightly tuning Φ or α (e.g. by a top gate on the junction), we can realize a large variety of holonomic qubit transformations that can densely cover a large part of the Bloch sphere, in the sense that with enough revolutions we can approach any point in the Bloch sphere as much as needed. (This observation is based on numerical evidence, and a rigorous demonstration is left for future work). Optimal coverage is achieved for $2\pi R\lambda_z^{-1} = 1$, see dashed red line in Fig. 3(a-d), resulting in the gray trajectory in Fig. 3(e). This kind of single-parameter holonomic manipulation is a peculiar possibility of the SASQ, and is a result of the long distances that the soliton state can travel in units of the SO length in a realistic device. A similar result for the particular case of $\lambda_z^{-1} = 0$ was obtained by Golovach *et al.* [23] in the context of holonomic spin manipulations of a small quantum dot electrostatically transported around a circle. Alternative modes of holonomic SASQ manipulation using two or more control parameters are, of course, also possible by combining ϕ control with variations of other device parameters such as k_F , v_F , or α .

Non-holonomic effects.—Up until now our analysis has predicted spin-degenerate soliton states, which are on the other hand a requirement for ideal holonomic operation of the SASQ. However, spin degeneracy is not guaranteed by any fundamental symmetry of our system (note that Krammer’s theorem [39, 40] does not apply, since time reversal symmetry is broken by the magnetic flux). Spin degeneracy in our model appears to be a consequence of the linear dispersion, even with finite SO coupling. If the dispersion acquires a finite curvature, the spin degeneracy is generally broken for finite α , creating a finite spin splitting $\delta\epsilon^\alpha$ in the qubit subspace. A Zeeman effect from the magnetic field, albeit weak, would also contribute to $\delta\epsilon^\alpha$ (with equal or opposite sign). The spin splitting $\delta\epsilon^\alpha$ imposes a lower bound on the velocity of holonomic qubit operations. If the gate frequency is below $\delta\epsilon/\hbar$, the holonomic orbit will acquire a non-holonomic (dynamic) “drift” that depends on the driving frequency.

To compute the $\delta\epsilon^\alpha$ splitting we introduce curvature in the dispersion by replacing $v_F(\nu k_\varphi - k_F - \nu A_\varphi)$ in Eq. (1) with $-W \cos[(k_\varphi - \nu A_\varphi)a_0] - \mu$, i.e., the dispersion of a tight-binding description of an effective mass model for the junction electrons. Here a_0 is the tight-binding

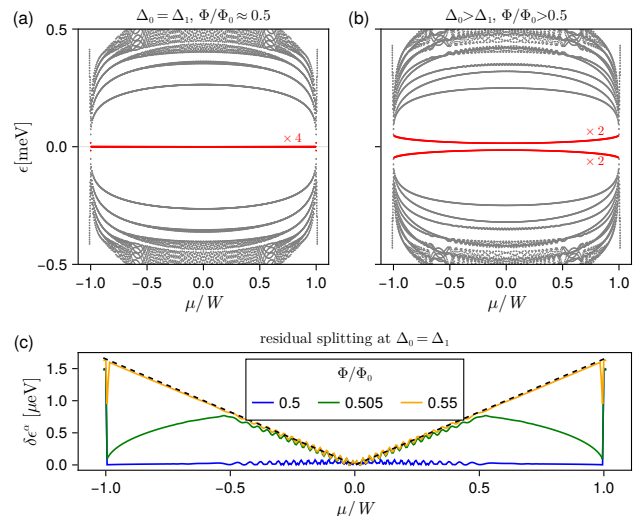


FIG. 4. (a,b) Spectrum of a SASQ versus chemical potential μ measured from the center of a band with cosine-like dispersion, half-bandwidth W and SO coupling $\alpha = 3$ meV nm. In (a), $\Delta_0 = \Delta_1 = 0.2$ meV and $\Phi/\Phi_0 \approx 0.50$. In (b) $\Delta_0 = 0.25$ meV, $\Delta_1 = 0.2$ meV and $\Phi/\Phi_0 = 0.85$. Shared parameters are $W = 30$ meV, $a_0 = 6.3$ nm and $R = 1\mu\text{m}$. (c) The non-linear dispersion and finite α produce a small spin splitting $\delta\epsilon^\alpha$ between solitonic levels [superimposed red curves in (a,b)]. Colored curves are different values of Φ/Φ_0 for $\Delta_0 = \Delta_1$. At $\Phi/\Phi_0 \approx 0.5$ and at half-filling $\mu = 0$, the residual splitting vanishes. The dashed line is the analytical expression Eq. (7). For $\Delta_0 \neq \Delta_1$, the splitting behaves similarly to the orange curve, matching the analytic result (not shown).

lattice spacing, $W = 1/(ma_0^2)$ is the half-bandwidth, m is the effective mass and μ is the chemical potential measured from half-filling. The spectrum of the junction as a function of μ across the full band is shown in Fig. 4(a,b) for two sets of representative model parameters with a finite $\alpha = 3\text{meV nm}$. For the special case $\Delta_0 = \Delta_1$ and $\Phi/\Phi_0 \approx 0.5$ in panel (a) the two $\nu = \pm 1$ level pairs coalesce into a four-fold quasi-degenerate solitonic mode at zero energy across the band. In all cases, the spin splitting of the solitonic levels is small, and cannot be resolved at the meV scales shown. In Fig. 4(c) we show the splitting $\delta\epsilon^\alpha$ at zoomed-in μeV scales for several fluxes and $\Delta_0 = \Delta_1$. For flux $\Phi/\Phi_0 = 0.55$ (orange line) and higher fluxes, the splitting is found to be described rather accurately (up to a superimposed oscillation around the band center) by the following formula (dashed black line)

$$\delta\epsilon^\alpha \approx \frac{\alpha}{R} \frac{\Phi}{\Phi_0} \frac{|\mu|}{W}. \quad (7)$$

However, at smaller fluxes approaching $\Phi/\Phi_0 = 0.5$ from above (green and blue curves), the splitting is suppressed.

Two main results may be drawn. First, the residual splitting due to dispersion curvature effects in the SASQ is upper-bounded by the scale α/R , which is in the

$\sim 1\mu\text{eV}$ scale for micron-sized junctions (GHz frequencies), although actual splittings can be much smaller. And second, the residual splitting and non-holonomic effects are completely suppressed when either Φ/Φ_0 approaches 0.5 or the density of states at the Fermi energy becomes flat, as corresponds to half filling in the above model, and to the linear dispersion in the model of Eq. (1).

To conclude, we have proposed a new type of superconducting qubit based on a Corbino JJ. A fluxoid mismatch across the junction induced by a weak magnetic flux confines a solitonic Andreev state that can be manipulated holonomically through a phase or voltage bias across the junction, which shuttles the soliton state around the disk. Holonomic trajectories are found to densely cover the Bloch sphere with a single control parameter. Non-holonomic modes of operation are also possible through dispersion-curvature effects by tuning the carrier density of the qubit. Soliton state shuttling in real space offers intriguing opportunities to engineer switchable couplings

and two-qubit gates between several qubits placed side by side [23]. It also allows detection schemes of the soliton state motion using e.g. a quantum point contact at some position close to the outer SASQ perimeter. The simplicity of the device, the lenient requirements regarding magnetic fields and SO couplings, and the maturity of available techniques to grow shallow, epitaxially proximitized quantum wells make the SASQ an appealing system to explore in future experiments.

ACKNOWLEDGMENTS

We thank Fernando Barbero for his help with mathematical aspects of this work and Charles Marcus for his insights about single-parameter operations. This research was supported by Grants PID2021-122769NB-I00 and PID2021-125343NB-I00 funded by MICIU/AEI/10.13039/501100011033, “ERDF A way of making Europe” and “ESF+”.

-
- [1] J. Koch, T. M. Yu, J. Gambetta, A. A. Houck, D. I. Schuster, J. Majer, A. Blais, M. H. Devoret, S. M. Girvin, and R. J. Schoelkopf, Charge-insensitive qubit design derived from the cooper pair box, *Phys. Rev. A* **76**, 042319 (2007).
- [2] J. A. Schreier, A. A. Houck, J. Koch, D. I. Schuster, B. R. Johnson, J. M. Chow, J. M. Gambetta, J. Majer, L. Frunzio, M. H. Devoret, S. M. Girvin, and R. J. Schoelkopf, Suppressing charge noise decoherence in superconducting charge qubits, *Phys. Rev. B* **77**, 180502 (2008).
- [3] C. Dickel, *Scalability and modularity for transmon-based quantum processors*, Dissertation, Delft University of Technology (2018).
- [4] S. B. Bravyi and A. Y. Kitaev, Fermionic quantum computation, *Annals of Physics* **298**, 210 (2002).
- [5] C. Nayak, S. Simon, A. Stern, M. Freedman, and S. Das Sarma, Non-abelian anyons and topological quantum computation, *Rev. Mod. Phys.* **80**, 1083 (2008).
- [6] S. D. Sarma, M. Freedman, and C. Nayak, Majorana zero modes and topological quantum computation, *Npj Quantum Information* **1**, 15001 EP (2015).
- [7] C. T. Hann, K. Noh, H. Putterman, M. H. Matheny, J. K. Iverson, M. T. Fang, C. Chamberland, O. Painter, and F. G. S. L. Brandão, Hybrid cat-transmon architecture for scalable, hardware-efficient quantum error correction, *PRX Quantum*, (2025).
- [8] H. Putterman *et al.*, Hardware-efficient quantum error correction via concatenated bosonic qubits, *Nature* **638**, 927 (2025).
- [9] C. D. Bruzewicz, J. Chiaverini, R. McConnell, and J. M. Sage, Trapped-ion quantum computing: Progress and challenges, *Appl. Phys. Rev.* **6**, 021314 (2019).
- [10] M. V. G. Dutt, L. Childress, L. Jiang, E. Togan, J. Maze, F. Jelezko, A. S. Zibrov, P. R. Hemmer, and M. D. Lukin, Quantum register based on individual electronic and nuclear spin qubits in diamond, *Science* **316**, 1312 (2007).
- [11] P. Kok, W. J. Munro, K. Nemoto, T. C. Ralph, J. P. Dowling, and G. J. Milburn, Linear optical quantum computing with photonic qubits, *Rev. Mod. Phys.* **79**, 135 (2007).
- [12] L. Casparis, M. R. Connolly, M. Kjaergaard, N. J. Pearson, A. Kringhøj, T. W. Larsen, F. Kuemmeth, T. Wang, C. Thomas, S. Gronin, G. C. Gardner, M. J. Manfra, C. M. Marcus, and K. D. Petersson, Superconducting gatemon qubit based on a proximitized two-dimensional electron gas, *Nature Nanotechnology* **13**, 915 (2018).
- [13] M. H. Devoret, A. Wallraff, and J. M. Martinis, Superconducting qubits: A short review (2004).
- [14] R. Seoane Souto and R. Aguado, Subgap states in semiconductor-superconductor devices for quantum technologies: Andreev qubits and minimal majorana chains (Springer Nature Switzerland, Cham, 2024) pp. 133–223.
- [15] A. Y. Kitaev, Unpaired majorana fermions in quantum wires, *Phys. Usp.* **44**, 131 (2001).
- [16] J. D. Sau and S. D. Sarma, Realizing a robust practical majorana chain in a quantum-dot-superconductor linear array, *Nature Communications* **3**, 964 (2012).
- [17] C. Padurariu and Y. V. Nazarov, Theoretical proposal for superconducting spin qubits, *Phys. Rev. B* **81**, 144519 (2010).
- [18] M. Hays, V. Fatemi, D. Bouman, J. Cerrillo, S. Diamond, K. Serniak, T. Connolly, P. Krogstrup, J. Nygård, A. L. Yeyati, A. Geresdi, and M. H. Devoret, Coherent manipulation of an andreev spin qubit, *Science* **373**, 430 (2021).
- [19] D. Loss and D. P. DiVincenzo, Quantum computation with quantum dots, *Phys. Rev. A* **57**, 120 (1998).
- [20] V. N. Golovach, M. Borhani, and D. Loss, Electric-dipole-induced spin resonance in quantum dots, *Phys. Rev. B* **74**, 165319 (2006).
- [21] D. V. Bulaev and D. Loss, Electric dipole spin resonance for heavy holes in quantum dots, *Phys. Rev. Lett.* **98**, 097202 (2007).

- [22] P. San-Jose, B. Scharfenberger, G. Schön, A. Shnirman, and G. Zarand, Geometric phases in semiconductor spin qubits: Manipulations and decoherence, *Phys. Rev. B* **77**, 045305 (2008).
- [23] V. N. Golovach, M. Borhani, and D. Loss, Holonomic quantum computation with electron spins in quantum dots, *Phys. Rev. A* **81**, 022315 (2010).
- [24] P. Zanardi and M. Rasetti, Holonomic quantum computation, *Physics Letters A* **264**, 94 (1999).
- [25] J. Zhang, T. H. Kyaw, S. Filipp, L.-C. Kwok, E. Sjöqvist, and D. Tong, Geometric and holonomic quantum computation, *Physics Reports* **1027**, 1 (2023).
- [26] J. C. Budich, D. G. Rothe, E. M. Hankiewicz, and B. Trauzettel, All-electric qubit control in heavy hole quantum dots via non-abelian geometric phases, *Phys. Rev. B* **85**, 205425 (2012).
- [27] S. Arroyo-Camejo, A. Lazariiev, S. W. Hell, and G. Bala-subramanian, Room temperature high-fidelity holonomic single-qubit gate on a solid-state spin, *Nature Communications* **5**, 4870 (2014).
- [28] P.-G. De Gennes, *Superconductivity of metals and alloys* (CRC Press, 2018).
- [29] For simplicity we have assumed the limit of a thin junction and ring. Away from this limit, one should distinguish between the average junction radius R , average ring radius R_1 and maximum disk radius R_0 , together with their respective fluxes, thicknesses and coherence lengths, to determine the relative values of A_φ , pairings Δ_0 and Δ_1 and fluxoids n as a function of field B_z . Increasing the difference between R_0 and R_1 would actually enlarge the B_z range for which a mismatch between disk and ring fluxoids is a stable minimum of the full free energy of the junction. Such microscopic considerations are left for future work.
- [30] F. London, *Superfluids*, Vol. 1 (Wiley, New York, 1950).
- [31] M. Tinkham, *Introduction to superconductivity* (Courier Corporation, 2004).
- [32] Closely related to this form of pairing interference is the fluxoid valve effect, recently predicted in full-shell nanowires [41]. There, it was shown that a cylindrically symmetric JJ will have a zero critical current when the two sides of the junction have different fluxoids. The same analysis applies to our circular junction.
- [33] Note that we have neglected here the flux-dependence of the pairings Δ_0 and Δ_1 , since they are not essential for the properties of the qubit, as long as they do not vanish (the so-called non-destructive Little-Parks regime [42, 43]).
- [34] X.-L. Qi, T. L. Hughes, and S.-C. Zhang, Chiral topological superconductor from the quantum hall state, *Phys. Rev. B* **82**, 184516 (2010).
- [35] X.-L. Qi and S.-C. Zhang, Topological insulators and superconductors, *Rev. Mod. Phys.* **83**, 1057 (2011).
- [36] R. Jackiw and C. Rebbi, Solitons with fermion number 1/2, *Phys. Rev. D* **13**, 3398 (1976).
- [37] P. San-Jose, G. Zarand, A. Shnirman, and G. Schön, Geometrical spin dephasing in quantum dots, *Phys. Rev. Lett.* **97**, 076803 (2006).
- [38] P. San-Jose, G. Schön, A. Shnirman, and G. Zarand, Spin dephasing due to a random berry phase, *Physica E* **40**, 76 (2007).
- [39] F. Zhang, C. L. Kane, and E. J. Mele, Time-reversal-invariant topological superconductivity and majorana kramers pairs, *Phys. Rev. Lett.* **111**, 056402 (2013).
- [40] H. Tasaki, *Physics and mathematics of quantum many-body systems*, Graduate texts in physics (Springer, Cham, 2020).
- [41] C. Payá, F. Matute-Cañadas, A. L. Yeyati, R. Aguado, P. San-Jose, and E. Prada, Fluxoid valve effect in full-shell nanowire josephson junctions, preprint arXiv:2504.16989 (2025).
- [42] W. A. Little and R. D. Parks, Observation of quantum periodicity in the transition temperature of a superconducting cylinder, *Phys. Rev. Lett.* **9**, 9 (1962).
- [43] D. Sabonis, O. Erlandsson, A. Kringhøj, B. van Heck, T. W. Larsen, I. Petkovic, P. Krogstrup, K. D. Petersson, and C. M. Marcus, Destructive little-parks effect in a full-shell nanowire-based transmon, *Phys. Rev. Lett.* **125**, 156804 (2020).